Stabilizing oscillation death by multicomponent coupling with mismatched delays

Wei Zou,[1,2,3,*] D. V. Senthilkumar,[3] Yang Tang,[2,3,4] and Jürgen Kurths[2,3,5]

[1]*School of Mathematics and Statistics, Huazhong University of Science and Technology, Wuhan 430074, China*

[2]*Institute of Physics, Humboldt University Berlin, Berlin D-12489, Germany*

[3]*Potsdam Institute for Climate Impact Research, Telegraphenberg, Potsdam D-14415, Germany*

[4]*Research Institute of Intelligent Control and Systems, Harbin Institute of Technology, Harbin 150080, China*

[5]*Institute for Complex Systems and Mathematical Biology, University of Aberdeen, Aberdeen AB24 3FX, United Kingdom*

(Received 24 April 2012; revised manuscript received 6 July 2012; published 20 September 2012)

The dynamics of a symmetric network of oscillators that are mutually coupled via multiple dynamical components with mismatched delays is studied. We find that networked oscillators experience oscillation death (OD) over a much larger domain of parameters when their different dynamical components are linked with mismatched delays than with only one delay. In particular, if the delays are mismatched by retaining a certain bias, OD is proved to be linearly stable even for very large delays for an arbitrary symmetric network. Further, we show that the minimal value of the intrinsic frequency necessary to induce OD decreases as the degree of mismatch in the coupling delays increases. The stabilizing effect of multicomponent coupling with mismatched delays is shown to be valid in networked chaotic oscillators also. The proposed coupling strategy can possibly be applied in controlling several pathological activities in neuronal systems and in engineering applications.

DOI: 10.1103/PhysRevE.86.036210 PACS number(s): 05.45.Xt, 87.10.−e

I. INTRODUCTION

The dynamics of nonlinear time-delayed complex systems has been a major focus in the field of nonlinear physics [1,2], where the presence of time delays gives rise to a plethora of intriguing collective behaviors. Among them oscillation death (OD), an interesting phenomenon of oscillation quenching in coupled nonlinear oscillators, has received continuous interest for two decades. OD was initially believed to occur only in coupled mismatched oscillators [3]. On the contrary, Ramana Reddy *et al*. [4,5] found that delayed coupling can induce OD even in coupled identical oscillators. Since then delay-induced OD has attracted considerable attention from researchers both experimentally and theoretically [6–23].

Recent investigations have revealed several novel delay-induced phenomena such as OD, chimera states, and phase-flip bifurcations, among others. [2]. Connection or feedback delays have been considered widely only in single-component coupling for simplicity, although multicomponent coupling is more realistic [24–26]. In most real-world systems, information transfer takes place in more than a single channel, e.g., multipath propagation with multiple delays is proposed to improve the efficiency in active sensing problems [27], in self-excited oscillators such as electrodynamics [28], in network-controlled systems [29], in controlling dynamical systems [30,31], and in pathological disorders [1]. Further, information transfer between neurons in the central nervous system is always realized through different axons of various lengths, which requires multicomponent coupling with nonidentical connection delays as an intrinsic property for better understanding of such systems from the point of view of dynamics. This more realistic form of coupling with multiple components and mismatched delays may provide a valuable step towards analyses of systems with more complex organization, and studies of complexity are rather topical currently [32,33].

To the best of the authors' knowledge, most studies about delay-induced OD have so far been restricted only to coupled nonlinear oscillators with a single coupling channel, with either symmetric or asymmetric delays between oscillators. For example, Prasad *et al*. found numerically and analytically that delay-induced OD is fairly general in two chaotic oscillators coupled by a single variable with symmetric delays [14,15]. Vicente *et al*. showed that the phenomenon of "death by delay" persists for a wide parameter range in a system of two mutually coupled semiconductor lasers with asymmetric delays, and death islands are characterized only by the average of two asymmetric delays between units [34,35]. Zou and Zhan reported that OD islands greatly expand along the coupling strength direction if a partial time-delay coupling is incorporated in a sufficiently large number of globally coupled oscillators, while OD islands in the two-oscillator case are also found to be determined only by the mean of the asymmetric delays between the two oscillators [18]. Punetha *et al*. focused particularly on a phase-flip transition within the OD regime of two coupled oscillators with asymmetric delays, where the importance of the average of the two delays is also considered [36].

In this contribution, we introduce an additional delayed coupling in a network of nonlinear oscillators which are coupled with their neighbors by multiple dynamical components with mismatched delays; see Fig. 1 for a schematic representation of the proposed coupling scheme. It should be noticed that the coupling delays are symmetric between the oscillators, but are mismatched, contributing to different propagation speeds through different channels. Such a network of delay-coupled oscillators are shown to experience OD for a much larger set of parameters than in the case of a single delay. Especially for a suitable interval of coupling strengths and with a certain mismatch of the coupling delays, OD is stable for any large delay, independently of the network size and topology. Further, the spread of the OD region increases with increasing intrinsic

*zouwei2010@mail.hust.edu.cn

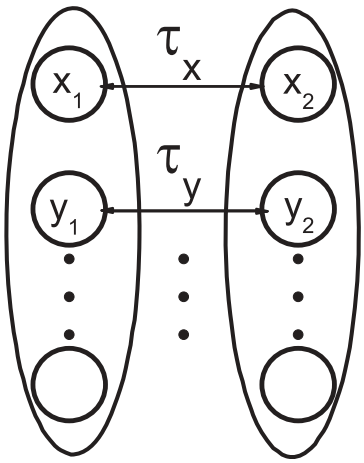

FIG. 1. Schematic representation of the coupling scheme used in this paper. Oscillators are connected to their neighbors through multiple dynamical variables with different coupling delays.

frequency, and the minimal value of the intrinsic frequency necessary to induce OD decreases as the degree of mismatch in the coupling delays is increased.

The rest of this paper is structured as follows. In the next section, the proposed coupling method is applied to networked Stuart-Landau oscillators. By adopting this standard limit-cycle model, we can provide a general insight into how the phenomenon of delay-induced OD arises in coupled oscillators where the oscillations are generated through a Hopf bifurcation. The numerical verification of the generality of this coupling scheme is then briefly demonstrated in Sec. III within a framework of networked chaotic Rössler oscillators. Finally the paper concludes with a discussion and summary in Sec. IV.

II. NETWORKED LIMIT-CYCLE OSCILLATORS

First, we present results for the paradigmatic Stuart-Landau oscillator [37]:

$$\dot{z} = (1 + iw - |z|^2)z, \tag{1}$$

where w is the intrinsic frequency of a single oscillator and $z = x + iy$ is a complex variable. This model represents a standard limit-cycle oscillator undergoing a supercritical Hopf bifurcation. It has an attracting limit cycle $z = e^{iwt}$ and an unstable focus located at the origin $z = 0$. Consider a symmetric network of N such oscillators coupled by two components x and y with mismatched delays; then the dynamics of the network is explicitly given in Cartesian coordinates as

$$\begin{aligned}\dot{x}_j &= p_j x_j - w y_j + \frac{K}{d_j}\sum_{s=1,s\neq j}^{N} g_{js}[x_s(t-\tau_x) - x_j],\\ \dot{y}_j &= w x_j + p_j y_j + \frac{K}{d_j}\sum_{s=1,s\neq j}^{N} g_{js}[y_s(t-\tau_y) - y_j],\end{aligned} \tag{2}$$

where $p_j = 1 - x_j^2 - y_j^2$ and $j = 1,\ldots,N$. Here $K > 0$ is the overall coupling strength, and τ_x and τ_y are two mismatched delays associated with the variables x and y. The network topology is encoded by g_{js} as follows: if oscillator j is linked to oscillator s, then $g_{js} = g_{sj} = 1$, otherwise $g_{js} = g_{sj} = 0$. Self-links are forbidden, i.e., $g_{jj} = 0$. $d_j = \sum_{s=1}^{N} g_{js}$ is the degree of node j.

A. Linear stability analysis of OD

To identify a stable OD state, the coupled oscillators Eq. (2) are linearized around the origin,

$$\begin{aligned}\dot{\xi}_{x,j} &= (1-K)\xi_{x,j} - w\xi_{y,j} + \frac{K}{d_j}\sum_{s=1,s\neq j}^{N} g_{js}\xi_{x,s}(t-\tau_x),\\ \dot{\xi}_{y,j} &= w\xi_{x,j} + (1-K)\xi_{y,j} + \frac{K}{d_j}\sum_{s=1,s\neq j}^{N} g_{js}\xi_{y,s}(t-\tau_y),\end{aligned} \tag{3}$$

where $\xi_{x,j}$ and $\xi_{y,j}$ are small perturbations. Using $\zeta = (\xi_{x,1},\xi_{y,1},\ldots,\xi_{x,N},\xi_{y,N})^T$ and denoting $G = (\frac{g_{js}}{d_j})_{N\times N}$, Eq. (3) can be rewritten as

$$\dot{\zeta} = (I_N \otimes A)\zeta + K(G\otimes B)\zeta(t-\tau_x) + K(G\otimes C)\zeta(t-\tau_y). \tag{4}$$

Here I_N denotes an N-dimensional identity matrix, $A = \begin{pmatrix} 1-K & -w \\ w & 1-K\end{pmatrix}$, $B = \begin{pmatrix} 1 & 0\\ 0 & 0\end{pmatrix}$, and $C = \begin{pmatrix} 0 & 0\\ 0 & 1\end{pmatrix}$.

The network matrix G can be diagonalized as $\Gamma^{-1}G\Gamma = \mathrm{diag}(\rho_1,\rho_2,\ldots,\rho_N)$ [11,18]. ρ_k $(k = 1,\ldots,N)$ are the eigenvalues of G, which are ordered as $1.0 = \rho_1 \geqslant \rho_2 \geqslant \cdots \geqslant \rho_{N-1} \geqslant -\frac{1}{N-1} \geqslant \rho_N \geqslant -1.0$. With the transformation of $\eta = (\Gamma\otimes I_2)\zeta$, G in Eq. (4) can be diagonalized to result in the following N block linear equations:

$$\begin{aligned}\dot{\eta}_{x,k} &= (1-K)\eta_{x,k} - w\eta_{y,k} + K\rho_k\eta_{x,k}(t-\tau_x),\\ \dot{\eta}_{y,k} &= w\eta_{x,k} + (1-K)\eta_{y,k} + K\rho_k\eta_{y,k}(t-\tau_y).\end{aligned} \tag{5}$$

By applying the ansatz $(\eta_{x,k},\eta_{y,k}) = ce^{\lambda t}$, $c\in\mathbf{R}^2$, we get N characteristic eigenvalue equations:

$$(1 - K + K\rho_k e^{-\lambda\tau_x} - \lambda)(1 - K + K\rho_k e^{-\lambda\tau_y} - \lambda) + w^2 = 0. \tag{6}$$

The coupled oscillator network of Eq. (2) experiences OD if and only if the largest real part $\lambda_{R,\max}$ of the roots λ of Eq. (6) is negative for every ρ_k $(k = 1,\ldots,N)$. The presence of delays τ_x and τ_y designates Eq. (6) as a transcendental equation, which has infinitely many (both complex and real) roots with negative real parts. However, there exists a finite number of roots with positive real parts attributed to instability.

Generally the roots of Eq. (6) cannot be expressed explicitly in terms of elementary functions. For two identical delays $\tau_x = \tau_y$, using the Lambert function W, which is the inverse function of $g(\Lambda) = \Lambda e^{\Lambda}$ for complex Λ [38], the roots of Eq. (6) can be solved analytically as

$$\lambda = \frac{1}{\tau_x}W(\tau_x K\rho_k e^{-\tau_x(1\pm iw)+\tau_x K}) + 1 \pm iw - K. \tag{7}$$

For two mismatched delays $\tau_x \neq \tau_y$, it is impossible to derive an analytical expression for the characteristic roots λ of Eq. (6). However, those roots can be computed numerically by employing pseudospectral differentiation techniques [39,40].

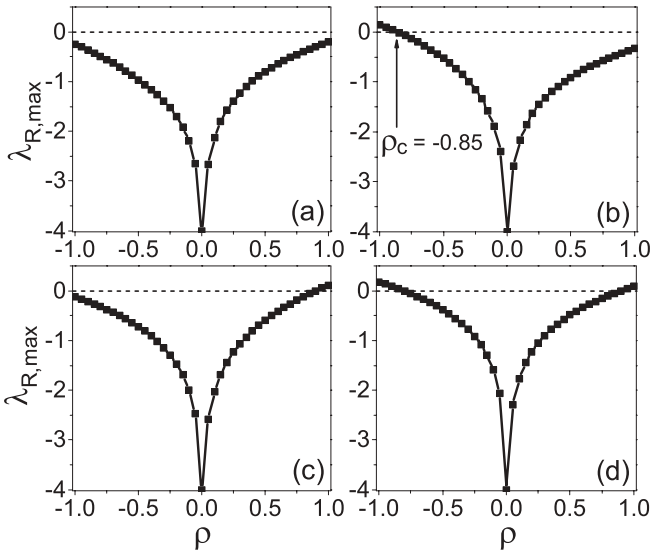

FIG. 2. Four typical dependences of the largest real part $\lambda_{R,\max}$ on the network eigenvalue ρ for networked Stuart-Landau oscillators Eq. (2). (a) ($\tau_x = 0.6$, $\tau_y = 1$), OD is stable for all symmetric networks. (b) ($\tau_x = 0.4$, $\tau_y = 1$), OD is stable for networks only if the smallest network eigenvalue $\rho_N > \rho_c = -0.85$. OD is unstable for any networks in (c) ($\tau_x = 0.5, \tau_y = 1$) and in (d) ($\tau_x = 1, \tau_y = 1$), as in both cases $\lambda_{R,\max}(\rho = 1) > 0$. $K = 5$ and $w = 10$ are fixed.

Since all networks have the common eigenvalue $\rho_1 = 1$, a necessary requirement to produce OD in the coupled oscillator network of Eq. (2) is $\lambda_{R,\max}(\rho_1 = 1) < 0$, which in turn implies that for some chosen parameter sets if $\lambda_{R,\max}(\rho_1 = 1) > 0$, OD will be unstable independently of the network topology. For the sake of clarification, we deal with the network eigenvalues ρ_k as a control parameter $\rho \in [-1,1]$ in Eq. (6). Figures 2(a)–2(d) show four types of the largest real part $\lambda_{R,\max}$ as a function of ρ for different τ_x, where $\tau_y = 1$, $K = 5$, and $w = 10$ are fixed. We find $\lambda_{R,\max} < 0$ for all $-1 \leqslant \rho \leqslant 1$ in Fig. 2(a), i.e., OD is stable irrespective of the network topology. In Fig. 2(b) OD is stable only for networks with $\rho_N > \rho_c = -0.85$. OD is unstable for any networks in Figs. 2(c) and 2(d), as the basic requisite condition $\lambda_{R,\max}(\rho = 1) < 0$ fails.

We also notice that $\lambda_{R,\max}$ monotonically increases as $|\rho|$ increases as shown in Fig. 2. This behavior holds generically for other choices of the parameters, and has already been analytically established for identical delays $\tau_x = \tau_y$ [13]. This observation leads to the fact that the stability of OD in an arbitrary symmetric network is finally defined only by the two extreme network eigenvalues: ρ_1 ($\rho_1 = 1$) and ρ_N ($-\frac{1}{N-1} \geqslant \rho_N \geqslant -1.0$). Two types of network with $\rho_N = -1$ and $\rho_N = 0$ provide, respectively, the lower and upper bounds for stable OD regions for arbitrary symmetric networks of coupled oscillators. These networks are in fact realized widely [12], e.g., all bipartite networks, such as chain networks, star networks, grid networks, and tree networks, possess $\rho_N = -1$, while for sufficiently large all-to-all networks $\rho_N \to 0$.

B. OD regions in the parameter space

Figures 3(a) and 3(b) plot the lower-bounded and upper-bounded stability regions of OD on the (τ_x, τ_y) plane, respectively. Combinations of τ_x and τ_y for stable OD are denoted in black. $w = 10$ and $K = 5$ are fixed. The lower-bounded OD region is well contained in the upper-bounded OD region. Interestingly, we observe that the identical delays $\tau_x = \tau_y$ induce OD only for a very limited interval of small delays (black regions along the diagonal), whereas two mismatched delays $\tau_x \neq \tau_y$ can cause OD over much wider regions with large delays (black strips parallel to the diagonal). The perfect symmetry of the OD regions along the diagonal on the (τ_x, τ_y) plane comes from the specially symmetric structure of the Stuart-Landau model.

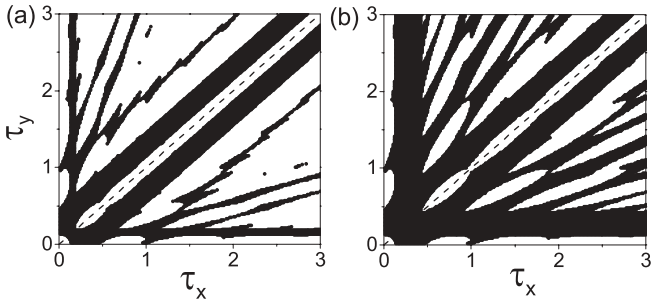

FIG. 3. The two limiting shapes of stable OD regions of Eq. (2) in the parameter space (τ_x, τ_y) for all symmetric networks: (a) lower-bounded region with $\rho_N = -1$ and (b) upper-bounded region with $\rho_N = 0$. Combinations of the two delays τ_x and τ_y, where OD sets in, are marked in black. $K = 5$ and $w = 10$ are fixed.

It is known from the above discussions that the OD regions depend on the values of the two extreme eigenvalue $\rho_1 = 1$ and ρ_N, while the smallest eigenvalues ρ_N are calculated from the matrix G which reflects the topology of the network. If the two delays retain a certain bias (mismatch), with the parameters located in the lower-bounded OD regime [Fig. 3(a)], for which $\lambda_{R,\max}(\rho) < 0$ holds for both $\rho_1 = 1$ and ρ_N, we can directly deduce that OD occurs independently of the network size and topology. The general structure of the stable OD region is retained for all networks with diverse topologies.

Figure 4 provides three illustrations of a ring network, an irregular (small-world-like) network, and an all-to-all network. The size of the networks is fixed at $N = 16$. The irregular network is constructed by randomly adding short or long edges on a initial ring network. The schematic representations of these network topologies are shown in Figs. 4(a)–4(c), and their smallest eigenvalues ρ_N turn out to be -1, -0.9124, and -0.0667, respectively. Their corresponding OD regions in the (τ_x, τ_y) plane are shown in Figs. 4(d)–4(f), respectively. The OD region shown in Fig. 4(d) is exactly the same as the lower-bounded OD region [Fig. 3(a)], as the smallest eigenvalue of ring networks with even nodes is always fixed at $\lambda_N = -1$ [12,20]. The OD region of the irregular network shown in Fig. 4(e) is clearly located between the lower-bounded and the upper-bounded OD regimes, where the structure of the lower-bounded OD regime shown in Fig. 3(a) persists. The smallest eigenvalue for an all-to-all network can be analytically obtained as $\lambda_N = -\frac{1}{N-1}$ [12,20]. In Fig. 4(f), we find that the OD region is nearly the same as the upper-bounded OD region [Fig. 3(b)], as $\lambda_N \to 0$ for large sizes of all-to-all networks.

In our numerical experiments, we have also studied many other types of network with different topologies. It comes out

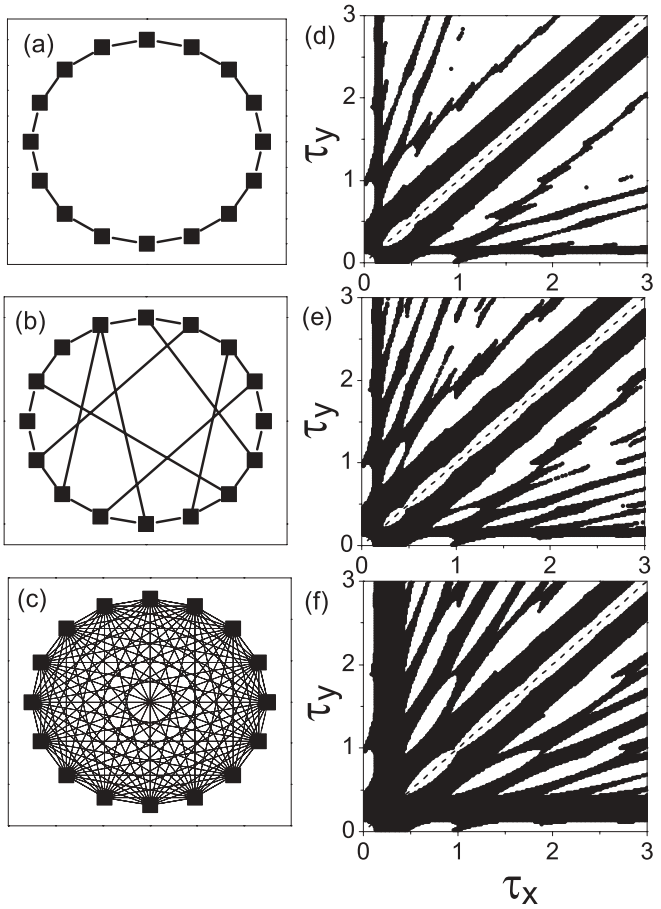

FIG. 4. Some illustrations of OD regions of Eq. (2) in the parameter space (τ_x,τ_y) for three different network topologies. Left column: (a)–(c) Sketch of topologies of the networks. The ρ_N's are -1, -0.9124, and -0.0667, respectively. Right column: (d)–(f) The corresponding OD regions of the networks (a)–(c). Combinations of the two delays τ_x and τ_y, where OD sets in, are marked in black. $K = 5$ and $w = 10$ are fixed.

that the OD regions are clearly between the lower-bounded and the upper-bounded OD regimes, and the structure of the lower-bounded OD region persists in the OD regions for all considered networks. Especially for both the small-world and scale-free networks with a large size, interestingly we observe that the OD regions are nearly the same as the upper-bounded OD regime [Fig. 3(b)], although their smallest eigenvalues ρ_N's are different. Figures 5(a) and 5(b) provide OD regions in the parameter space (τ_x,τ_y) for a small-world network with the rewiring probability $p = 0.1$ [41] and a scale-free network with the scaling exponent $\gamma = 3$ [42]. The size of both complex networks is $N = 1000$, and their respective smallest eigenvalues are $\rho_N \approx -0.6661$ and $\rho_N \approx -0.7359$. We find that the OD regions in Figs. 5(a) and 5(b) are indeed identical to the upper-bounded OD regime [Fig. 3(b)]. The OD regions in the parameter space stay nearly the same as the upper-bounded OD regime and do not sensitively dependent on the complex network structure; a similar effect has been observed in the case of a single delay [20].

To understand this interesting phenomenon in complex networks, we have depicted the values of $\lambda_{R,\max}$ versus τ_x for

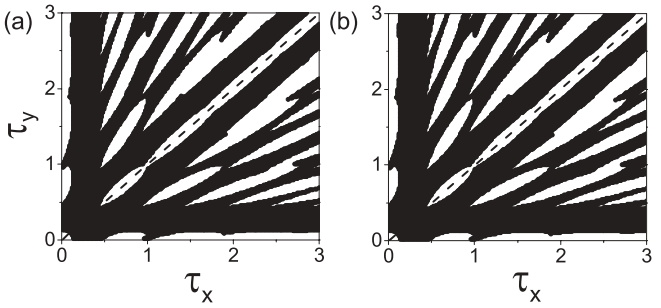

FIG. 5. OD regions of Eq. (2) in the parameter space (τ_x,τ_y) for (a) a small-world network with the rewiring probability $p = 0.1$ and (b) a scale-free network with the scaling exponent $\gamma = 3$. The size of both complex networks is $N = 1000$. Their smallest eigenvalues are $\rho_N = -0.6661$ for (a) and $\rho_N = -0.7359$ for (b). Combinations of the two delays τ_x and τ_y, where OD sets in, are marked in black. $K = 5$ and $w = 10$ are fixed.

$\rho = 1, -0.6661$, and -0.7359 with $\tau_y = \tau_x + 0.2$ in Fig. 6(a) and $\tau_y = \tau_x + 1.0$ in Fig. 6(b) for the parameters $K = 5$ and $w = 10$. We find that both $\lambda_{R,\max}(\rho = 1) > \lambda_{R,\max}(\rho = -0.6661)$ and $\lambda_{R,\max}(\rho = 1) > \lambda_{R,\max}(\rho = -0.7359)$ hold for nearly all values of the parameter τ_x. Thus the OD regions are determined only by the largest eigenvalue $\rho_1 = 1$ (i.e., the upper-bounded OD region), although the smallest eigenvalues ρ_N's are different. In fact, with many other realizations of small-world and scale-free networks, it is generically observed that $\lambda_{R,\max}(\rho_1 = 1) > \lambda_{R,\max}(\rho_N)$ holds for most of the parameters. This observation accounts for the phenomenon of OD regions of complex networks observed in Fig. 5.

By relating the two delays with a bias as $\tau_y = \tau_x + \alpha$, the lower-bounded stable OD region in the (K,τ_x) plane for different values of α is depicted in Fig. 7 for $w = 10$ and $\rho_N = -1$. When $\alpha = 0$ (one single delay), only a single narrow death island, in which OD occurs, is formed in the parameter space [Fig. 7(a)]. As α increases from zero, the death island is deformed and enlarged [Fig. 7(b)], and then more islands appear [Figs. 7(c) and 7(d)]. If α is beyond a critical value $\alpha > \alpha_c$ ($\alpha_c \approx 0.11$), all death islands merge into a single large connected region. The stability region is unbounded in the τ_x direction for a certain range of the coupling strength K. This behavior persists for $0.12 \leqslant \alpha \leqslant 0.45$ [Figs. 7(e)–7(g)]. Further increase in α ($\alpha > 0.45$) results in a stability region consisting of several disjointed and bounded sets [Figs. 7(h) and 7(i)], which is valid for all larger values of α. The

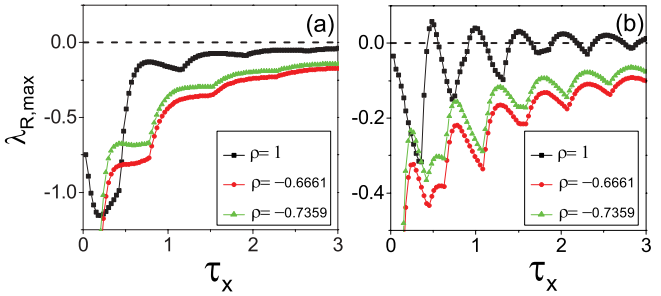

FIG. 6. (Color online) $\lambda_{R,\max}$ versus τ_x for $\rho = 1, -0.6661$, and -0.7359. (a) $\tau_y = \tau_x + 0.2$ and (b) $\tau_y = \tau_x + 1.0$. $K = 5$ and $w = 10$ are fixed.

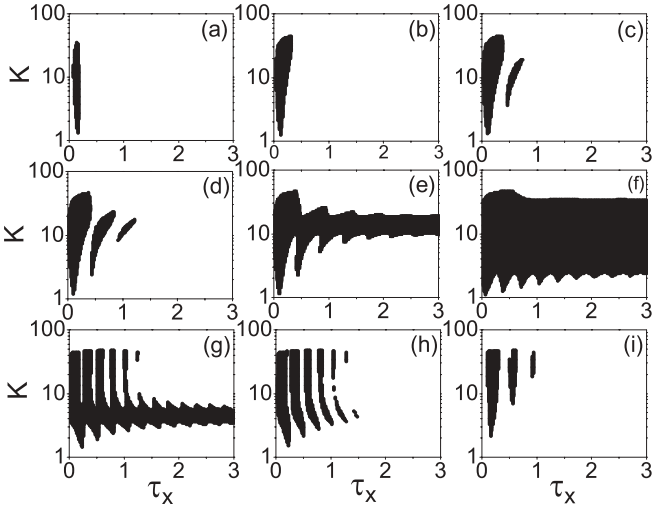

FIG. 7. Variation of the lower-bounded stable OD regions of Eq. (2) in the parameter space (τ_x, K) as the mismatch α of delays increases, where the two delays are related as $\tau_y = \tau_x + \alpha$. (a) $\alpha = 0$, (b) $\alpha = 0.08$, (c) $\alpha = 0.1$, (d) $\alpha = 0.11$, (e) $\alpha = 0.12$, (f) $\alpha = 0.2$, (g) $\alpha = 0.45$, (h) $\alpha = 0.46$, and (i) $\alpha = 0.72$. Parameters at which OD sets in are marked in black. $w = 10$ is fixed.

mechanism behind the enhancement in the spread of OD can be intuitively understood as follows. It is well established that a single feedback delay can induce OD for suitable parameter values. The additional (extra) degrees of freedom introduced by the mismatched parameter α of the second delay and the phase shift introduced by them cause the annihilation of the oscillatory behavior for a larger set of parameters. However, much more detailed investigations are necessary; this remains an open problem.

It should be noted that similar unbounded OD regimes along the delay direction as in Figs. 7(e)–7(g) have been reported by Atay in two coupled Stuart-Landau oscillators, but with uniformly distributed delays, if the variance of the delay distribution is beyond a threshold [11]. Compared with the above-mentioned work, here we have obtained the unbounded regimes of OD in an arbitrary oscillator network with just two discrete delays, which holds only for a certain interval of mismatch of two delays. Our approach opens up the possibility of an easy way to experimentally realize the observed phenomenon in a laboratory. In addition, the OD regimes are also shown to be greatly enlarged in the parameter space constructed by two coupling delays associated with different dynamical variables.

C. OD by two large mismatched delays

To deepen the understanding of this stabilizing effect of two mismatched delays, Figs. 8(a) and 8(b) compare the dependence of $\lambda_{R,\max}(\rho = 1,-1)$ on τ_x for two identical, $\tau_y = \tau_x$, and mismatched, $\tau_y = \tau_x + 0.2$, delays for $w = 10$ and $K = 5$, respectively. In Fig. 8(a), the range of τ_x marked by I denotes the lower-bounded stable OD region, where the value of $\lambda_{R,\max}$ is negative for both $\rho = 1$ and $\rho = -1$; and the range II stands for the upper bound, within which the value of $\lambda_{R,\max}$ is negative for $\rho = 1$, and $\lambda_{R,\max}(\rho = 0) = 1 - K = -4 < 0$ already holds. For large values of τ_x, $\lambda_{R,\max}(\rho = 1,-1)$ always stays positive, and a power law $\lambda_{R,\max}(\rho = 1,-1) \propto \frac{1}{\tau_x}$ is observed if τ_x is large enough. The discontinuity of $\lambda_{R,\max}$ in Fig. 8(a) due to the points with negative values cannot be plotted on the log-log scale. In contrast, the value of $\lambda_{R,\max}(\rho = 1,-1)$ is negative for all τ_x in Fig. 8(b), and a power law relation of $\lambda_{R,\max}(\rho = 1,-1) \propto -\frac{1}{\tau_x}$ is revealed for sufficiently large τ_x, which implies that OD is linearly stable by two mismatched delays even for very large delays. Note that Fig. 8(b) is referring to $-\lambda_{R,\max}$.

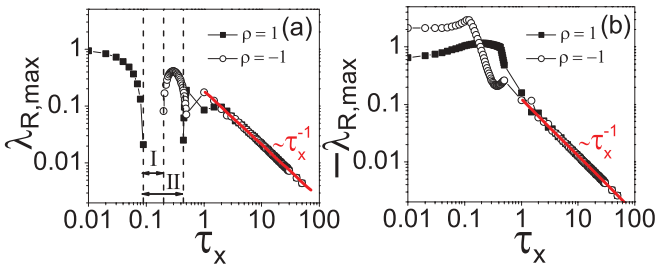

FIG. 8. (Color online) Comparison of the dependence of $\lambda_{R,\max}(\rho = 1,-1)$ on the delay τ_x for (a) two identical delays $\tau_y = \tau_x$ and (b) two mismatched delays $\tau_y = \tau_x + 0.2$. Ranges marked by I and II in (a) represent the smallest and largest stability ranges of the delay τ_x, respectively. The two red lines show two distinct power law relations: $\lambda_{R,\max}(\rho = 1,-1) \propto 1/\tau_x$ for (a) and $\lambda_{R,\max}(\rho = 1,-1) \propto -1/\tau_x$ for (b). $K = 5$ and $w = 10$ are fixed.

From the power law scaling in Fig. 8(b) we deduce that the phenomenon of OD is supposed to persist even for very large delays. Now, we further reveal that OD is linearly stable for a rather large interval of coupling strength in the limit of large coupling delays. Figure 9(a) first plots the function of $\lambda_{R,\max}(\rho = 1,-1)$ versus the coupling strength K for a large value of the delay $\tau_x = 30$, where the two delays are related as $\tau_y = \tau_x + 0.2$ and $w = 10$ is fixed. We find that the lower-bounded OD interval is $K_{c1} < K < K_{c2}$, where $K_{c1} \approx 2.5$ and $K_{c2} \approx 33$, within which $\lambda_{R,\max}(\rho = 1,-1) < 0$ holds. Surprisingly for $K_{c1} < K < K_{c2}$, the power-law-scaling relation of $\lambda_{R,\max}(\rho = 1,-1) \propto -\frac{1}{\tau_x}$ obtained in Fig. 8(b) is generically valid; as shown in Fig. 9(b) for $K = 3$, 20, and 30 with $\tau_y = \tau_x + 0.2$ and $w = 10$. This observation demonstrates that OD is stable even for very large delays for

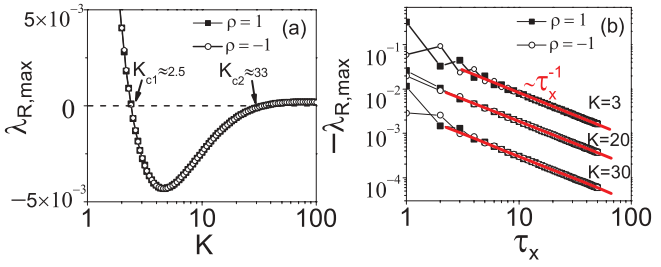

FIG. 9. (Color online) (a) $\lambda_{R,\max}(\rho = 1,-1)$ versus coupling strength K for $\tau_x = 30$. The lower-bounded OD region is $K_{c1} < K < K_{c2}$, where $K_{c1} \approx 2.5$ and $K_{c2} \approx 33$. (b) The power-law-scaling relation $\lambda_{R,\max}(\rho = 1,-1) \propto -1/\tau_x$ for different coupling strengths. The three red lines show the linear fittings of log-log plots. From top to bottom $K = 3$, 20, and 30, respectively. $\tau_y = \tau_x + 0.2$ and $w = 10$ are fixed.

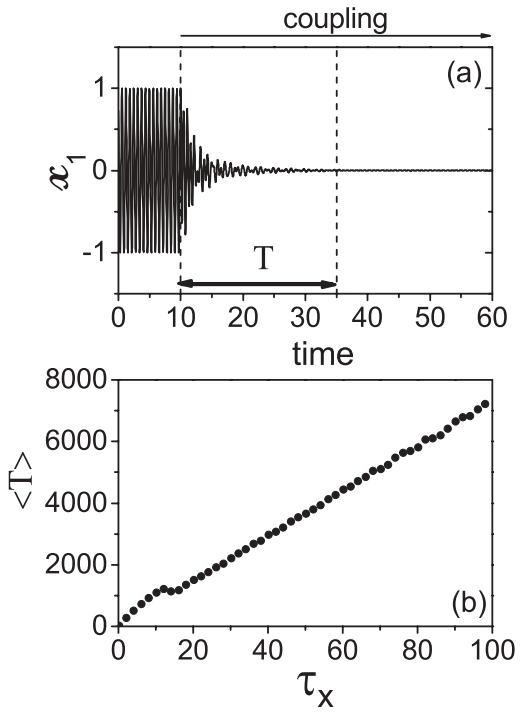

FIG. 10. (a) Time series x_1 for coupled Stuart-Landau oscillators Eq. (2) with $N = 2$ and $\tau_x = 1$, where T is the transient time for which both oscillators become death after the coupling is switched on at $t = 10$. (b) The average transient time $\langle T \rangle$ versus the delay τ_x, where each point has been averaged over 20 times with different random initial conditions. $\tau_y = \tau_x + 0.2$, $K = 5$, and $w = 10$ are fixed.

a certain large interval of the coupling strength. Note that Fig. 9(b) refers to $-\lambda_{R,\max}$.

At a first glance, it might seem surprising that OD persists even for very large delays, as if τ_x approaches infinity, $\tau_y = \tau_x + 0.2$ also approximates infinity. In the limit of infinite coupling delays of different variables between oscillators, the signals cannot reach other oscillators in finite time through all channels, which is akin to the absence of coupling. So the phenomenon of coupling-induced OD in such a case seems to be counterintuitive. To understand it, we numerically calculate the transient time needed for a pair of coupled Stuart-Landau oscillators to achieve OD after the coupling is switched on. Figure 10(a) illustrates the OD transient time T of the coupled systems Eq. (2) with $N = 2$, $\tau_x = 1$, and $\tau_y = \tau_x + 0.2$. The coupling is turned on after all the oscillators evolve freely for a long time with random initial conditions. In Fig. 10(b), we show the dependence of the averaged OD transient time $\langle T \rangle$ on τ_x, where each point has been averaged over 20 samples with different random initial conditions. There is indeed a clear tendency of monotonically increasing $\langle T \rangle$ with increasing τ_x. The larger the coupling delay τ_x, the longer is the OD transient time. For sufficiently large but finite coupling delays, the coupled systems are assumed to reach OD given a sufficiently long waiting time. Thus even if OD is proved to be linearly stable for very large delays, the coupled systems cannot experience OD in finite time.

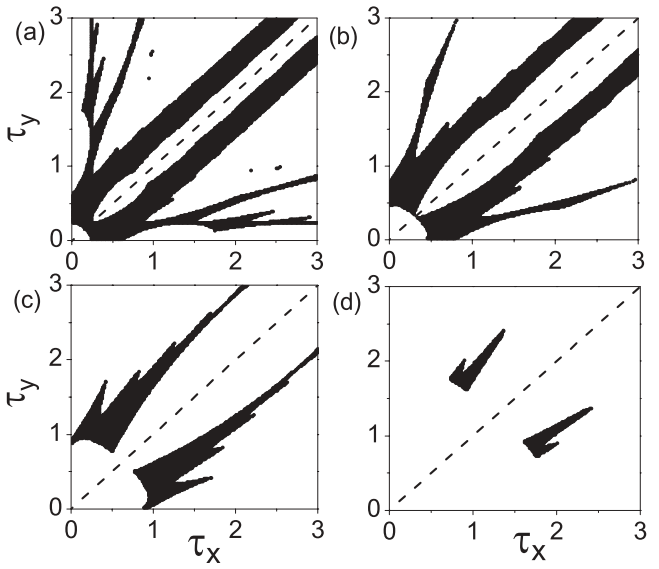

FIG. 11. The lower-bounded stable OD region of Eq. (2) in the parameter space (τ_x, τ_y) monotonically decreasing as the natural frequency w decreases. (a) $w = 7$, (b) $w = 5$, (c) $w = 4$, and (d) $w = 3.5$. Parameters with which OD sets in are marked in black. $K = 5$ is fixed.

D. Effects of the intrinsic frequency w on OD

The intrinsic frequency w determines the characteristic time scales $\frac{2\pi}{w}$ of a single Stuart-Landau oscillator, which has been verified to play a crucial role in inducing OD in coupled oscillators with both discrete [4,5] and distributed [11] time delays. Next we explore the role of w in the OD region of coupled systems (2). Figures 11(a)–11(d) depict OD regions in the parameter space (τ_x, τ_y) for four different values of w, where the coupling strength $K = 5$ is fixed. We observe that the multicomponent coupling with mismatched delays is capable of not only enhancing the onset of OD in a large set of parameters, but also inducing OD where there is no OD at all for identical delays when w is very low; see the OD regions shown in Figs. 11(c) and 11(d) for $w = 4$ and 3.5. The OD region in the parameter space (τ_x, τ_y) monotonically decreases with decreasing w.

Figures 12(a)–12(d) depict OD regions in the parameter space (τ_x, K) for $w = 8, 7.5, 7$, and 6, respectively, where $\tau_y = \tau_x + 0.2$. With decreasing w from 8 to 7.5, the unbounded OD region [Fig. 12(a)] splits into several disjointed and bounded OD islands [Fig. 12(b)]. With further decreasing w, the number of OD islands decreases [Figs. 12(c) and 12(d)]. OD islands completely vanish in the parameter space (τ_x, K) if w is smaller than a certain threshold $w_{\min}$.

The value of $w_{\min} = 4.812$ has been reported by Reddy *et al.* for two identical delays $\tau_x = \tau_y$ [5]. Mismatched delays $\tau_x \neq \tau_y$ can induce OD even when the intrinsic frequency w is lower than this value, which can be deduced from the OD regions shown in Figs. 11(c) and 11(d) for $w = 4$ and 3.5. By gradually increasing α in $\tau_y = \tau_x + \alpha$, we numerically compute the values of $w_{\min}$ and the results are shown in Fig. 13, from which we find that $w_{\min}$ monotonically decreases with increasing α. Thus the proposed coupling

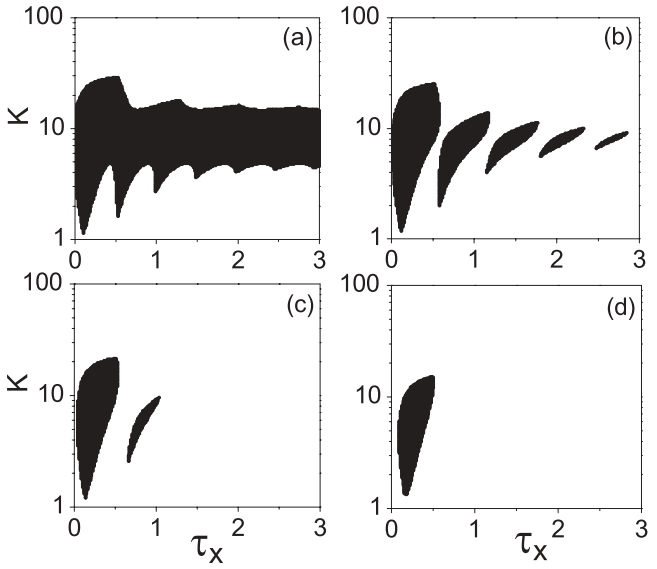

FIG. 12. The lower-bounded stable OD region of Eq. (2) in the parameter space (τ_x, K) monotonically decreasing as the nature frequency w decreases. (a) $w = 8$, (b) $w = 7.5$, (c) $w = 7$, and (d) $w = 6$. Parameters at which OD sets in are marked in black. The two delays are related as $\tau_y = \tau_x + 0.2$.

scheme also facilitates delay-induced OD through the intrinsic frequency w.

III. NETWORKED CHAOTIC OSCILLATORS

The stability effect of multicomponent coupling with mismatched delays on OD not only holds for a network of limit-cycle oscillators, but is also valid for a network of chaotic oscillators. For example, let us consider a network of chaotic Rössler oscillators linked to their neighboring nodes in the same manner as in the networked limit-cycle oscillators of Eq. (2). The network of delay-coupled chaotic Rössler oscillators is represented as

$$\dot{x}_i = -y_i - z_i + \frac{K}{d_i} \sum_{j=1, j\neq i}^{N} g_{ji}[x_j(t-\tau_x) - x_i],$$

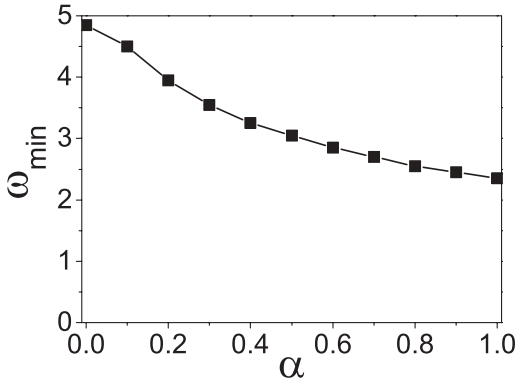

FIG. 13. The minimum value $w_{\min}$ of w for which OD is possible in the parameter space (τ_x, K), decreasing as the mismatch α of delays increases, where the two delays are related as $\tau_y = \tau_x + \alpha$.

$$\dot{y}_i = x_i + a y_i + \frac{K}{d_i} \sum_{j=1, j\neq i}^{N} g_{ji}[y_j(t-\tau_y) - y_i], \quad (8)$$
$$\dot{z}_i = b + z_i(x_i - c),$$

where $i = 1,2,\ldots,N$. The parameter set $(a = 0.15, b = 0.2, c = 10)$ is chosen such that the single Rössler oscillator behaves chaotically, and has an unstable focus $P = (x^*, y^*, z^*)$ with $x^* = -a y^*$, $y^* = -z^*$, and $z^* = \frac{c-\sqrt{c^2-4ab}}{2a}$. OD is realized in the network of chaotic Rössler oscillator, Eq. (8), by stabilizing the unstable fixed point P for suitable coupling strength.

By performing a standard linear stability of Eq. (8) around the fixed point P, the following characteristic equations are obtained, which determine the stability of OD:

$$\begin{vmatrix} K\rho_k e^{-\lambda\tau_x} - K - \lambda & -1 & -1 \\ 1 & a + K\rho_k e^{-\lambda\tau_y} - K - \lambda & 0 \\ z^* & 0 & x^* - c - \lambda \end{vmatrix} = 0, \quad (9)$$

where the ρ_k's $(k = 1,2,\ldots,N)$ are the network eigenvalues and $|M|$ denotes the determinant of the matrix M. Here the detailed procedure is not provided because it is quite similar to that in Sec. II. The roots of Eq. (9) are numerically computed with the same techniques used to solve Eq. (6). Figures 14(a)–14(d) plot four typical dependences of the largest real part $\lambda_{R,\max}$ of Eq. (9) on the network eigenvalue ρ. The structures are the same as those in Figs. 2(a)–2(d), which means that the lower and upper bounds for stable OD regions of networks of chaotic Rössler oscillators are also given by the OD regimes of networks with $\rho_N = -1$ and $\rho_N = 0$, respectively.

We depict the lower-bounded and upper-bounded stability regions of OD in the parameter space of (τ_x, τ_y) in Figs. 15(a) and 15(b), respectively. Combinations of the two delays τ_x and τ_y for which the fixed point P is successfully stabilized (i.e., OD occurs) are indicated by black. The coupling strength is

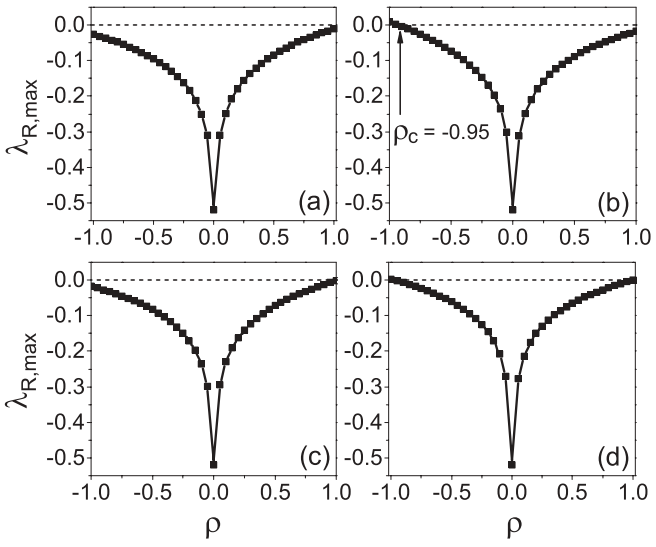

FIG. 14. Four typical dependences of the largest real part $\lambda_{R,\max}$ of Eq. (9) on the network eigenvalue ρ for networked Rössler oscillators. (a) $(\tau_x = 2.5, \tau_y = 10)$, (b) $(\tau_x = 3.5, \tau_y = 10)$, (c) $(\tau_x = 5.5, \tau_y = 10)$, and (d) $(\tau_x = 9.5, \tau_y = 10)$. $K = 1$.

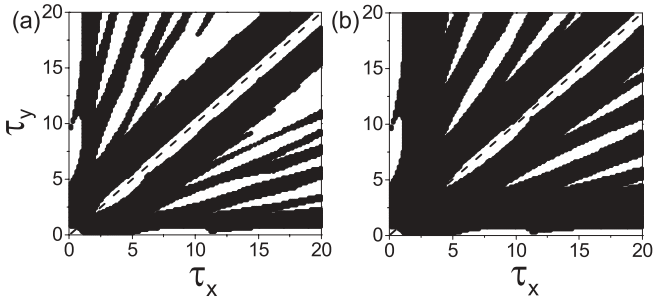

FIG. 15. (a), (b) Lower-bounded and upper-bounded stable OD regions in the parameter space (τ_x, τ_y) for networked chaotic Rössler oscillators of Eq. (8), where the oscillators are coupled by two dynamical components x and y with mismatched delays τ_x and τ_y. $K = 1$.

fixed at $K = 1$. The structures of the two limited stable OD regions closely resemble those shown in Figs. 3(a) and 3(b), which confirms the generality that stabilization of OD with our proposed coupling scheme of mismatched delays is much more effective than in the case of a single identical delay. Note that both the lower-bounded and upper-bounded stable OD regions are no longer strictly symmetric with respect to the diagonal. In our numerical experiments using coupled Eq. (8) with diverse networks, the obtained OD regions are found to be clearly located between the lower-bounded and upper-bounded OD stability regions.

IV. CONCLUSIONS AND DISCUSSION

In conclusion, we have proposed a more realistic form of delayed coupling in networked oscillators, where neighboring oscillators are coupled by multiple components with mismatched delays. It is found that by using mismatched delays the stability region of OD can be drastically enlarged. By relating mismatched delays with a certain bias, OD is proved to be linearly stable even for very large delays irrespective of the network size and topology. Further, we have shown that the minimal value of the intrinsic frequency necessary to induce OD decreases as the degree of mismatch in the delay is increased. The generality of this stabilizing effect of mismatched delays on OD is underscored by considering networked chaotic Rössler oscillators.

Control of unstable steady states in delayed-feedback oscillators has been a topic of extensive research in chaos control recently [1]. As the proposed coupling method is also accessible for stabilization of an isolated oscillator, it seems to have strong potential to be exploited in controlling complex networks, pathological activities such as Parkinson's disease, epilepsy, etc., in neuroscience and in engineering applications. One direct extension in future is to use this coupling scheme to stabilize unstable periodic orbits of dynamical systems by choosing all the mismatched delays of the dynamical components to be integer multiples of the period of the target orbit. Finally, we believe our proposed coupling scheme in this work will be interesting for the wide physical community.

ACKNOWLEDGMENTS

This work was supported by the Alexander von Humboldt Foundation of Germany, the National Natural Science Foundation of China (Grants No. 11147179, No. 11202082, and No. 61203235), the Fundamental Research Funds for the Central Universities of China under Grant No. 2011QN161, the SUMO (EU), the PHOCUS (EU), and IRTG1740 (DFG-FAPESP). We thank two anonymous reviewers for their thoughtful comments which greatly improved this work.

[1] *Handbook of Chaos Control*, edited by E. Schöll and H. G. Schuster, 2nd completely revised and enlarged ed. (Wiley-VCH, Weinheim, 2008).
[2] M. Lakshmanan and D. V. Senthilkumar, *Dynamics of Nonlinear Time-Delay Systems* (Springer, Berlin, 2010).
[3] D. G. Aronson, G. B. Ermentrout, and N. Kopell, Physica D **41**, 403 (1990).
[4] D. V. Ramana Reddy, A. Sen, and G. L. Johnston, Phys. Rev. Lett. **80**, 5109 (1998).
[5] D. V. Ramana Reddy, A. Sen, and G. L. Johnston, Physica D **129**, 15 (1999).
[6] D. V. Ramana Reddy, A. Sen, and G. L. Johnston, Phys. Rev. Lett. **85**, 3381 (2000).
[7] A. Takamatsu, T. Fujii, and I. Endo, Phys. Rev. Lett. **85**, 2026 (2000).
[8] R. Herrero, M. Figueras, J. Rius, F. Pi, and G. Orriols, Phys. Rev. Lett. **84**, 5312 (2000).
[9] S. H. Strogatz, Nature (London) **394**, 316 (1998).
[10] R. Dodla, A. Sen, and G. L. Johnston, Phys. Rev. E **69**, 056217 (2004).
[11] F. M. Atay, Phys. Rev. Lett. **91**, 094101 (2003).
[12] F. M. Atay, J. Diff. Eqns. **221**, 190 (2006).
[13] M. P. Mehta and A. Sen, Phys. Lett. A **355**, 202 (2006).
[14] A. Prasad, Phys. Rev. E **72**, 056204 (2005).
[15] A. Prasad, J. Kurths, S. K. Dana, and R. Ramaswamy, Phys. Rev. E **74**, 035204(R) (2006).
[16] K. Konishi, Phys. Rev. E **70**, 066201 (2004).
[17] K. Konishi, H. Kokame, and N. Hara, Phys. Rev. E **81**, 016201 (2010).
[18] W. Zou and M. Zhan, Phys. Rev. E **80**, 065204(R) (2009).
[19] W. Zou, C. G. Yao, and M. Zhan, Phys. Rev. E **82**, 056203 (2010).
[20] W. Zou, X. Zheng, and M. Zhan, Chaos **21**, 023130 (2011).
[21] W. Zou, J. Q. Lu, Y. Tang, C. J. Zhang, and J. Kurths, Phys. Rev. E **84**, 066208 (2011).
[22] W. Zou, Y. Tang, L. X. Li, and J. Kurths, Phys. Rev. E **85**, 046206 (2012).
[23] C. G. Yao, W. Zou, and Q. Zhao, Chaos **22**, 023149 (2012).
[24] T. Lindvall, *Lectures on the Coupling Method* (Wiley, New York, 1992).
[25] H. Thorisson and T. Lindvall, *Coupling, Stationarity, and Regeneration* (Springer, New York, 2000).
[26] I. Ugi, Pure Appl. Chem. **73**, 187 (2001).

[27] A. Balanov, N. Janson, C. Wan, and M. Wiercigroch, report from the 43rd European Study Group with Industry, Lancaster, 2002 (unpublished).
[28] A. S. Ishchenko, Yu. V. Novozhilova, and M. I. Petelin, Radiophys. Quantum Electron. **49**, 485 (2006).
[29] F. L. Lian, J. Moyne, and D. Tilbury, Int. J. Control **76**, 591 (2003).
[30] A. Ahlborn and U. Parlitz, Phys. Rev. Lett. **93**, 264101 (2004).
[31] A. Ahlborn and U. Parlitz, Phys. Rev. E **72**, 016206 (2005).
[32] A. Arenas, A. Díaz-Guilera, J. Kurths, Y. Moreno, and C. Zhou, Phys. Rep. **469**, 93 (2008).
[33] M. E. J. Newman, Am. J. Phys. **79**, 800 (2011).
[34] R. Vicente, S. Tang, J. Mulet, C. R. Mirasso, and J.-M. Liu, Phys. Rev. E **70**, 046216 (2004).
[35] R. Vicente, S. Tang, J. Mulet, C. R. Mirasso, and J.-M. Liu, Phys. Rev. E **73**, 047201 (2006).
[36] N. Punetha, R. Karnatak, A. Prasad, J. Kurths, and R. Ramaswamy, Phys. Rev. E **85**, 046204 (2012).
[37] Y. Kuramoto, *Chemical Oscillations, Waves, and Turbulence* (Springer, Berlin, 1984).
[38] J. K. Hale, *Functional Differential Equations* (Springer, New York, 1971).
[39] D. Breda, Appl. Numer. Math. **56**, 305 (2006).
[40] D. Breda, S. Maset, and R. Vermiglio, Appl. Numer. Math. **56**, 318 (2006).
[41] D. J. Watts and S. H. Strogatz, Nature (London) **393**, 440 (1998).
[42] A.-L. Barabási and R. Albert, Science **286**, 509 (1999).